Substituent Effects and Bonding Characteristics in (o-Benzoquinone diimine)bis(bipyridine)ruthenium(II) Complexes

Hitoshi Masui, A. B. P. Lever,* and Elaine S. Dodsworth

Department of Chemistry, York University, North York (Toronto), Ontario, Canada M3J 1P3

Received May 19, 1992

The effect of substituents on the electrochemistry and electronic spectroscopy of $Ru^{II}(bpy)_2LL$ complexes is reported, where bpy = 2,2'-bipyridine and LL = 4,5-disubstituted *o*-benzoquinone diimines, *o*-semiquinone diimines, *o*-benzenediamides, and *o*-phenylenediamines. These data are used to create a map of the orbital energies as a function of the Hammett parameter of the substituents, giving insight into the electronic behavior of these complexes. Electronic spectra are characterized with respect to energy, intensity, and bandwidth, and bands are assigned with support from resonance Raman (rR) and FTIR data. The solvatochromism of the *o*-benzoquinone diimine species is discussed. The data are interpreted in the context of metal–ligand orbital mixing and electronic structure. An ab initio study of the uncomplexed ligand in its quinone diimine oxidation state is also included.

Introduction

Quinonoid ligands[1-19] and their analogues, the *o*-benzoquinone diimines,[20-39] are redox-active species that produce complexes in which mixing between metal and ligand orbitals can play an important role in determining the physical and chemical properties of the complexes. We have been interested in studying how the electronic structures of such complexes may be probed.[4-8,18,19] When there is considerable covalency between a redox-active metal center and a coordinated redox-active ligand, the assignment of oxidation states to the metal or to the ligand may be ambiguous. Such is the case for the (*o*-benzoquinone diimine)bis(bipyridine)-ruthenium(II) complex, which can be formally regarded as having a ruthenium(II) quinonoid electronic configuration but has some characteristics of a ruthenium(III) semiquinonoid species.[18,40]

The degree of covalency between the metal and ligand orbitals is a function of the energies, symmetries, and overlap of the valence metal and ligand orbitals. In this study, we were interested in determining how the electronic structure is affected by a change in the energy of the *o*-benzoquinone diimine valence orbital and by a change in the net oxidation state of this ligand.

The energies of the ligand orbitals were adjusted by attaching electron-donating or -withdrawing substituents onto the 4 and 5 positions of the quinonoid ring. Solvatochromic studies were also carried out to provide a means of assessing the charge-transfer character of the electronic transitions exhibited by these complexes. Resonance Raman (rR) and Fourier transform infrared (FTIR) vibrational data are also reported in support of our conclusions. The resulting shifts in the redox potentials and charge-transfer bands were interpreted using a molecular orbital analysis based on that reported by Magnuson and Taube.[41] Orbital energies are mapped as a function of the Hammett $\sum\sigma_p$ values of the substituents, in accordance with spectroscopic assignments, transition energies, and redox potentials of the complexes. We also include an ab initio study of the molecular orbital energies of the uncomplexed ligand in its quinonoid oxidation state.

The ligands in the *o*-benzoquinone diimine, *o*-semiquinone diimine, and *o*-benzenediamide oxidation states are designated R_2-bqdi (carrying no net charge), R_2-sqdi (carrying one negative charge), and R_2-opda (carrying two negative charges), respec-

(1) Kessel, S. L.; Emerson, R. M.; Debrunner, P. G.; Hendrickson, D. N. *Inorg. Chem.* **1980**, *19*, 1170.
(2) Bhattacharya, S.; Pierpont, C. G. *Inorg. Chem.* **1991**, *30*, 1511 and 2906. Bhattacharya, S.; Pierpont, C. G. *Inorg. Chem.* **1992**, *31*, 35 and references therein.
(3) Harmalker, S.; Jones, S. E.; Sawyer, D. T. *Inorg. Chem.* **1983**, *22*, 2790.
(4) Haga, M.-A.; Dodsworth, E. S.; Lever, A. B. P. *Inorg. Chem.* **1986**, *25*, 447.
(5) Stufkens, D. J.; Snoeck, Th. L.; Lever, A. B. P. *Inorg. Chem.* **1988**, *27*, 935.
(6) Lever, A. B. P.; Auburn, P. R.; Dodsworth, E. S.; Haga, M.-A.; Liu, W.; Melnik, M.; Nevin, W. A. *J. Am. Chem. Soc.* **1988**, *110*, 8076.
(7) Auburn, P. R.; Dodsworth, E. S.; Haga, M.; Liu, W.; Nevin, W. A.; Lever, A. B. P. *Inorg. Chem.* **1991**, *31*, 3502.
(8) Stufkens, D. J.; Snoeck, Th. L.; Lever, A. B. P. *Inorg. Chem.* **1988**, *27*, 953.
(9) Thompson, J. S.; Calabrese, J. C. *Inorg. Chem.* **1985**, *24*, 3167.
(10) Sofen, S. R.; Ware, D. C.; Cooper, S. R.; Raymond, K. N. *Inorg. Chem.* **1979**, *18*, 234.
(11) Boone, S. R.; Pierpont, C. G. *Inorg. Chem.* **1987**, *26*, 1769.
(12) Espinet, P.; Bailey, P. M.; Maitlis, P. M. *J. Chem. Soc., Dalton Trans.* **1979**, 1542.
(13) Pierpont, C. G.; Buchanan, R. M. *Coord. Chem. Rev.* **1981**, *38*, 45.
(14) Cooper, S. R.; Koh, Y. B.; Raymond, K. N. *J. Am. Chem. Soc.* **1982**, *102*, 5092.
(15) (a) Benelli, C.; Dei, A.; Gatteschi, D.; Pardi, L. *Inorg. Chem.* **1989**, *28*, 1476. (b) Benelli, C.; Dei, A.; Gatteschi, D.; Güdel, H. U.; Pardi, L. *Inorg. Chem.* **1989**, *28*, 3091. (c) Benelli, C.; Dei, A.; Gatteschi, D.; Pardi, L. *Inorg. Chem.* **1990**, *29*, 3409.
(16) Bruni, S.; Cariati, F.; Dei, A.; Gatteschi, D. *Inorg. Chim. Acta* **1991**, *186*, 157.
(17) Dei, A.; Gatteschi, D.; Pardi, L.; Barra, A. L.; Brunel, L. C. *Chem. Phys. Lett.* **1990**, *175*, 589. Dei, A.; Pardi, L. *Inorg. Chim. Acta* **1991**, *181*, 3.
(18) Masui, H.; Lever, A. B. P.; Auburn, P. A. *Inorg. Chem.* **1991**, *30*, 2402.
(19) Auburn, P. R.; Lever, A. B. P. *Inorg. Chem.* **1990**, *29*, 2551.
(20) Balch, A. L.; Holm, R. H. *J. Am. Chem. Soc.* **1966**, *88*, 5201.
(21) Baikie, P. E.; Mills, O. S. *Inorg. Chim. Acta* **1967**, *1*, 55.
(22) Duff, E. J. *J. Chem. Soc. A* **1968**, 434.
(23) Warren, L. F. *Inorg. Chem.* **1977**, *16*, 2814.
(24) Reinhold, J.; Benedix, R.; Birner, P.; Hennig, H. *Inorg. Chim. Acta* **1979**, *33*, 209.
(25) Vogler, A.; Kunkely, H. *Angew. Chem., Int. Ed. Engl.* **1980**, *19*, 221.
(26) Belser, P.; von Zelewsky, A.; Zehnder, M. *Inorg. Chem.* **1981**, *20*, 3098.
(27) El'Cov, A. V.; Maslennikova, T. A.; Kukuschkin, V. Ju.; Shavurov, V. V. *J. Prakt. Chem.* **1983**, *B325*, S27.
(28) Pyle, A. M.; Barton, J. K. *Inorg. Chem.* **1987**, *26*, 3820.
(29) Pyle, A. M.; Chiang, M. Y.; Barton, J. K. *Inorg. Chem.* **1990**, *29*, 4487.
(30) Thorn, D. L.; Hoffmann, R. *Nouv. J. Chim.* **1979**, *3*, 39.
(31) Peng, S.-M.; Chen, C.-T.; Liaw, D.-S.; Chen, C.-I.; Wang, Y. *Inorg. Chim. Acta* **1985**, *101*, L31.
(32) Christoph, G. G.; Goedken, V. L. *J. Am. Chem. Soc.* **1973**, *95*, 3869.
(33) Hall, G. S.; Soderberg, R. H. *Inorg. Chem.* **1968**, *7*, 2300.
(34) Gross, M. E.; Ibers, J. A.; Trogler, W. C. *Organometallics* **1982**, *1*, 530.
(35) Zehnder, M.; Loliger, H. *Helv. Chim. Acta* **1980**, *63*, 754.
(36) Danopoulos, A. A.; Wong, A. C. C.; Wilkinson, G.; Hursthouse, M. B.; Hussain, B. *J. Chem. Soc., Dalton Trans.* **1990**, 315.
(37) Nemeth, S.; Simandi, L. I.; Argay, G.; Kalman, A. *Inorg. Chim. Acta* **1989**, *166*, 31.
(38) Joss, S.; Hasselbach, K. M.; Buergi, H. B.; Wordel, R.; Wagner, F. E.; Ludi, A. *Inorg. Chem.* **1989**, *28*, 1815.
(39) Rieder, K.; Hauser, U.; Sieganthaler, H.; Schmidt, E.; Ludi, A. *Inorg. Chem.* **1975**, *14*, 1902.
(40) Carugo, O.; Djinovic, K.; Rizzi, M.; Castellani, C. B. *J. Chem. Soc., Dalton Trans.* **1991**, 1551.
(41) Magnuson, R. H.; Taube, H. *J. Am. Chem. Soc.* **1975**, *97*, 5129.

0020-1669/93/1332-0258$04.00/0

tively, where R denotes the substituent. The neutral *o*-phenylenediamine ligand is distinguished from the diamide form, where one proton has been removed from each amino group, by the abbreviations R_2-opdaH$_2$ and R_2-opda, respectively.

Experimental Section

Reagents. All of the commercially obtained *o*-phenylenediamine ligands were reagent grade or better and were used without further purification. Water was doubly distilled (the second time from potassium permanganate) and passed through Barnstead activated charcoal and ion-exchange filters. Solvents were dried and distilled by standard methods just prior to use.[42]

Physical Measurements. Electronic spectra were obtained on Cary Model 2400 and Hitachi-Perkin-Elmer Model 340 spectrometers. Nuclear magnetic resonance (NMR) spectra were recorded on a Bruker AM300 NMR spectrometer. The observed splittings of the NMR signals are described as singlets (s), doublets (d), triplets (t), or multiplets (m). Cyclic and differential pulse voltammograms were obtained using Princeton Applied Research Corp. (PARC) 173, 174, and 179 instrumentation at platinum wire electrodes in dry acetonitrile solutions containing 0.1 M tetrabutylammonium hexafluorophosphate ($TBAPF_6$). A AgCl-coated silver wire, separated from the bulk solution by a frit, served as a quasi-reference electrode, and ferrocene was added as an internal reference. Potentials are reported versus SCE, assuming the ferrocenium/ferrocene couple to be at 0.425 V vs SCE.[43] Spectroelectrochemistry was performed either in a Hartl cell[44] or in a 1-cm glass cuvette using acetonitrile solutions containing 0.3 M $TBAPF_6$, a platinum mesh working electrode, a nichrome wire counter electrode separated from bulk by a frit, and the aforementioned quasi-reference electrode. Substituent dependence studies were carried out in acetonitrile solutions except where otherwise stated.

Resonance Raman spectra in CH_2Cl_2 were recorded at the University of Amsterdam, using a Dilor XY resonance Raman spectrometer. These data were calibrated against solvent bands. A detailed discussion of these data, in relation to those of other similar compounds, will appear elsewhere.[45]

Ab initio calculations were performed using Spartan (Wavefunction Inc.) running on a Silicon Graphics Personal Iris computer. The geometry was optimized at the AM1 level, and the STO3b basis set was used.

Syntheses. 4,5-Dimethoxy-1,2-benzenediamine Monohydrochloride. The preparation of this compound has previously been reported;[46] however, better yields were obtained by the following method. To a solution of 4,5-dinitroveratrole[47] (0.500 g; 2.55 mmol) in concentrated HCl (10 mL) was added $SnCl_2 \cdot 2H_2O$ (3.27 g; 14.5 mmol). The mixture was stirred, in a closed container, for 16 h during which time the yellow solution became nearly colorless and some product precipitated from solution. Complete precipitation was achieved by saturating the reaction mixture with diethyl ether. The white, granular product was isolated by filtration, washed with 1:9 EtOH/H_2O, diethyl ether, and hexanes, and air dried. The product was recrystallized from a minimum amount of 5:1 EtOH/H_2O by the rapid addition of diethyl ether. Large, white plates crystallized within 15 min and were isolated by filtration. Yield = 90%. Anal. Calcd for $C_8H_{13}N_2O_2Cl$: C, 46.92; H, 6.40; N, 13.74. Found: C, 46.85; H, 6.42; N, 13.51.

$[Ru(bpy)_2(R_2\text{-opdaH}_2)](PF_6)_2$ (R = OMe, Me, H, Cl). These complexes were synthesized according to the following general procedure: Dichlorobis(bipyridine)ruthenium(II)[48] (0.100 g; 0.206 mmol) was suspended in 5 mL of methanol under a nitrogen atmosphere. To the suspension was added a 10% excess (1:1 stoichiometry) of the appropriate 4,5-disubstituted *o*-phenylenediamine. The mixture was refluxed for 16 h during which time the initial purple suspension was converted to a blood red solution. The solution was filtered under an inert atmosphere, and a deoxygenated solution containing NH_4PF_6 (0.3 g) in 5% aqueous acetic acid (5 mL) was added to the filtrate. The mixture was heated briefly to boiling and then allowed to cool slowly to room temperature. The resulting crystals were isolated by quick filtration in air, washed with small amounts of ice cold water and copious amounts of diethyl ether and hexanes, and dried in vacuo.

NMR data for the R = OMe complex in deuterated acetonitrile referenced to TMS: 3.78 (6, s), 4.79 (2, d), 5.43 (2, d), 6.80 (2, s), 7.20 (2, t), 7.63 (2, t), 7.69 (2, d), 7.84 (2, t), 8.13 (2, t), 8.34 (2, d), 8.50 (2, d), 8.71 (2, d).

$[Ru(bpy)_2(R_2\text{-bqdi})](PF_6)_2$ (R = Cl, H, Me). The synthetic procedure for the corresponding R_2-opdaH$_2$ complexes was followed until the blood-red solution was obtained. After cooling, concentrated ammonia (1.0 mL) was added to the solution and the mixture was bubbled with air until all of the solvent evaporated. The exposure to air deepens the color of the solution. The residue was redissolved in the minimum amount of methanol, and NH_4PF_6 (0.3 g) was added slowly to the solution as an aqueous solution of equal volume. The resulting precipitate was isolated and rinsed with ice water and copious amounts of diethyl ether and hexanes. Recrystallization was achieved by slowly cooling a hot, saturated, aqueous solution of the product.

$[Ru(bpy)_2(R_2\text{-bqdi})](PF_6)_2$ (R = NH_2, OMe). 1,2,4,5-Benzenetetramine tetrahydrochloride (Aldrich) was used in the synthesis of the diamino-substituted complex, while 4,5-dimethoxy-1,2-benzenediamine monohydrochloride (vide supra) was used in the synthesis of the dimethoxy-substituted complex. One equivalent of sodium acetate dihydrate per 1 equiv of ligand hydrochloride was added, in a nitrogen atmosphere, to a mixture containing dichlorobis(bipyridine)ruthenium and 10% excess (1:1 stoichiometry) of ligand in methanol (5 mL) to generate the neutral, free ligand in situ. Following the formation of a blood-red solution, the procedure was then continued as above.

The diamino-substituted complex was purified by Soxhlet extraction of the crude solid with dichloromethane. As the extract became concentrated, it yielded fine crystals of the product.

NMR data for R = NH_2 complex in deuterated acetone, referenced to TMS: 6.20 (s, 6), 7.49 (t, 2), 7.75 (t, 2), 7.84 (d, 2), 8.08 (t, 2), 8.21 (t, 2), 8.39 (d, 2), 8.70 (t, 4), 10.46 (s, 2).

NMR data for the R = OMe complex in deuterated acetonitrile referenced to TMS: 3.84 (6, s), 6.40 (2, s), 7.41 (2, t), 7.56 (4, m), 7.90 (2, d), 8.03 (2, t), 8.11 (2, t), 8.21 (4, d), 10.94 (2, s).

$[Ru(bpy)_2(NO_2\text{-bqdi})](PF_6)_2$. (N.B.: The NO_2-substituted ligand is monosubstituted in the 4 position whereas all other ligands are disubstituted in the 4 and 5 positions.) To a suspension of dichlorobis(bipyridine)-ruthenium(II) (0.1 g; 0.206 mmol) in methanol (5 mL) was added silver nitrate (0.070 g; 0.412 mmol). The mixture was stirred for 3 h and then filtered through a Celite bed. The blood-red filtrate was deoxygenated, placed under a nitrogen atmosphere, and treated with 4-nitro-1,2-benzenediamine (0.035 g; 0.228 mmol). The mixture was refluxed for 16 h and subsequently filtered. The filtrate was bubbled with air until the solvent evaporated. The resulting residue was further purified by chromatography on a silica column, eluting with a mixture containing 1:1 acetone/water and 1% w/v KCl. The largest fraction was collected and concentrated, and the product was precipitated by the addition of NH_4PF_6.

$[Ru(bpy)_2((NH_2)_2\text{-opdaH}_2)](PF_6)_2$. This complex was obtained by treating a saturated solution of the $(NH_2)_2$-bqdi complex in 10% aqueous acetic acid with zinc amalgam powder under an inert atmosphere. The solution was filtered to remove excess zinc amalgam, and the product was precipitated from the resulting orange-red filtrate by adding an excess of NH_4PF_6. Microcrystals were isolated by filtration under nitrogen and washed with small amounts of cold 10% acetic acid and copious amounts of diethyl ether and dried in vacuo.

N.B.: Sodium perchlorate (0.3 g) was used instead of NH_4PF_6 in some of the earlier syntheses and seems to produce better quality crystals, but the practice was discontinued for safety reasons.

Although the R_2-bqdi and R_2-opdaH$_2$ species were directly prepared and obtained as solid materials, the R_2-sqdi species were not isolated due their rapid oxidation in air. The spectroelectrochemical data for the R_2sqdi species were obtained by controlled-potential reduction of the R_2-bqdi species at a potential 100 mV negative of the first reduction wave.

Chemical Analyses. $[Ru(bpy)_2(bqdi)](PF_6)_2$. Anal. Calcd for $C_{26}H_{22}F_{12}N_6P_2Ru$: C, 38.58; H, 2.74; N, 10.38. Found: C, 38.78; H, 2.90; N, 10.10.

$[Ru(bpy)_2((NH_2)_2\text{-bqdi})](PF_6)_2 \cdot H_2O$. Anal. Calcd for $C_{26}H_{26}F_{12}N_8OP_2Ru$: C, 36.42; H, 3.06; N, 13.07. Found: C, 36.11; H, 2.91; N, 12.52.

(42) Perrin, D. D.; Armarego, W. L. F. *Purification of Laboratory Chemicals*, 3rd ed.; Pergamon Press plc.: London, 1988.
(43) Gennett, T.; Milner, D. F.; Weaver, M. J. *J. Phys. Chem.* **1985**, *89*, 2787.
(44) Krejcik, M.; Danek, M.; Hartl, F. *J. Electroanal. Chem.* **1991**, *317*, 179.
(45) Stufkens, D. J.; Snoeck, Th. L.; Dodsworth, E. S.; Masui, H.; Metcalfe, R. A.; Lever, A. B. P. To be submitted for publication.
(46) Nakamura, M.; Toda, M.; Saito, H.; Ohkura, Y. *Anal. Chim. Acta* **1982**, *134*, 39.
(47) Ehrlich, J.; Bogert, M. T. *J. Org. Chem.* **1947**, *12*, 522.
(48) Sullivan, B. P.; Salmon, D. J.; Meyer, T. J. *Inorg. Chem.* **1978**, *17*, 3334.

Table I. Ab Initio Orbital Energy Calculations of R_2-bqdi Ligands[a]

R	LUMO(π^*)	HOMO(π)	SHOMO[b,c]	THOMO(σ)[b]
4-NO_2	0.113 31	−0.271 67	−0.349 42	−0.361 80
4,5-Cl_2	0.116 39	−0.267 04	−0.358 72	−0.360 14
H	0.148 84	−0.244 04	−0.334 13	−0.358 10
4,5-Me_2	0.153 32	−0.231 67	−0.327 69	−0.344 66
4,5-$(OMe)_2$	0.155 35	−0.222 19	−0.292 70	−0.327 30
4,5-$(NH_2)_2$	0.173 37	−0.199 61	−0.260 23	−0.311 38

[a] Energies are in hartrees (1 hartree = 219 489 cm^{-1}). [b] Second (SHOMO) and third (THOMO) highest occupied molecular orbitals. [c] Orbital is of σ symmetry for R = NO_2, H, and Me and π for R = Cl, OMe, and NH_2.

[Ru(bpy)$_2$((CH$_3$)$_2$-bqdi)](PF$_6$)$_2$. Anal. Calcd for $C_{28}H_{26}F_{12}N_6P_2Ru$: C, 40.15; H, 3.13; N, 10.03. Found: C, 40.24; H, 3.44; N, 10.03.

[Ru(bpy)$_2$(Cl$_2$-bqdi)](PF$_6$)$_2$. Anal. Calcd for $C_{26}H_{20}Cl_2F_{12}N_6P_2Ru$: C, 35.55; H, 2.29; N, 9.57. Found: C, 35.47; H, 2.65; N, 9.47.

[Ru(bpy)$_2$((OCH$_3$)$_2$-opdaH$_2$)](ClO$_4$)$_2$. Anal. Calcd for $C_{28}H_{26}Cl_2N_6O_{10}Ru$: C, 43.20; H, 3.37; N, 10.79. Found: C, 43.02; H, 3.49; N, 10.68.

[Ru(bpy)$_2$(NO$_2$-bqdi)](PF$_6$)$_2$. Anal. Calcd for $C_{26}H_{21}F_{12}N_7O_2P_2Ru$: C, 36.55; H, 2.48; N, 11.47. Found: C, 37.31; H, 2.76; N, 11.75.

Summary of Resonance Raman Spectra. Data were collected in dichloromethane solution and are reported with peak energies in cm^{-1} and relative intensities in parentheses. $[Ru(bpy)_2(Cl_2\text{-bqdi})]^{2+}$ (excitation at 543 nm): 310 (0.13); 491 (0.12); 601 (1.0); 656 (0.21); 669 (0.25); 916 (0.087); 1200, 1218 (0.17); 1264 (0.11). $[Ru(bpy)_2(Cl_2\text{-sqdi})]^+$ (excitation at 515 nm): 604 (bqdi impurity); 665, 672 (0.8); 1169 (0.52); 1263 (0.35); [1314 (0.39)]; 1484 (1.0); [1517 (0.52)]; 1557 (0.52); 1604 (0.2). Peaks in brackets were not observed in all runs of this species and may arise from decomposition products. $[Ru(bpy)_2(Cl_2\text{-sqdi})]^+$ (excitation at 620 nm): 570 (1.0); 666 (0.3); 819 (0.1); 1140 (0.16); 1195 (0.41); 1352 (0.23); 1477 (0.35).

Summary of ν(Ru–N) FTIR Data. Data were collected using KBr pellets. Peak energies as follows are in cm^{-1}: R = NO_2 (monosubstituted in the 4 position, chloride salt), 556; R = Cl, 599; R = H, 620; R = Me, 603; R = OMe, 594; R = NH_2, 591.

Results and Discussion

A. Molecular Orbital Energy Level Diagram. In the discussion which follows, symmetry labels appropriate to the local C_{2v} point group are used. Ab initio calculations of the free ligand fragment show that the HOMO π level has a_2 symmetry (labeled a_2) and lies approximately 10 000 cm^{-1} above the SHOMO (second highest occupied MO), which is σ or π depending upon the substituent (Table I). The LUMO π^* has b_2 (labeled $2b_2^*$) symmetry. As discussed previously,[4,18] group theoretical methods lead to the simplified molecular orbital diagram (Figure 1), appropriate for the bqdi and sqdi oxidation states. The HOMO(π) and LUMO(π^*) of the bqdi ligand will couple to the metal (xy) $2a_2$ and (yz) b_2 orbitals, respectively, with the latter interaction being more important than the former due to a more favorable overlap. The remaining d(t_{2g}) orbital is (z^2) a_1 (in this framework; see Figure 1; orbitals rotated with axes) and has some σ^* character from interaction with the low-lying bqdi $9a_1$ orbital. The data below lead to the conclusion that the a_1 and $2a_2$ orbitals lie close together; for the purpose of the ensuing discussion they will be assumed to be of roughly equal energy. No evidence was observed for any transitions to the next higher (2nd) LUMO of the bqdi or sqdi species.

B. Electrochemistry. The cyclic voltammogram of a R_2-bqdi complex, displayed in Figure 2, shows five reversible or quasi-reversible ($i_a = i_c$) coulometrically determined one-electron redox processes. These were assigned previously[18,26] as shown in Table II. The two most negative processes (V, IV) correspond to the successive reduction of the bipyridine ligands; these have potentials only slightly dependent on the bqdi substituent.

The next three processes (III, II, I) formally correspond with R_2-sqdi/R_2-opda, R_2-bqdi/R_2-sqdi, and Ru^{III}/Ru^{II}. The potentials of these couples all depend upon the Hammett $\Sigma\sigma_p$ parameter of the bqdi substituent, as shown in Figure 3. All of the potentials become more positive as the electron-withdrawing ability of the substituent increases. Since the substituents are each both para and meta to quinonoid nitrogen donor atoms, we used a sum of the σ_p values for the R substituent.[49]

Indeed there is quite a large change in the donor character of the quinonoid ligand over this series of substituents. This is recognized from the values of the electrochemical parameter, E_L, for these species,[50] derived from the Ru^{III}/Ru^{II} potentials listed in Table II. These range from 0.38 for R = NO_2, similar to a phosphite, to 0.01 for R = NH_2, similar to a saturated amine. The electrochemistry of the opdaH_2 species exhibit irreversible redox processes with unusual features which will be discussed elsewhere.[51]

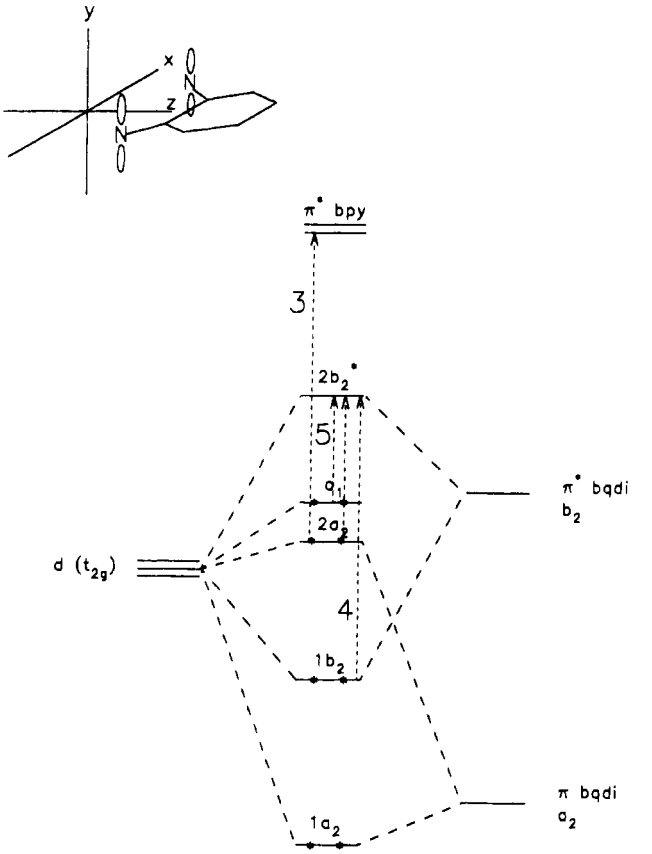

Figure 1. Simplified molecular orbital model of the R_2-bqdi and R_2-sqdi complexes. The transition labels correspond to the band labels of Figure 4.

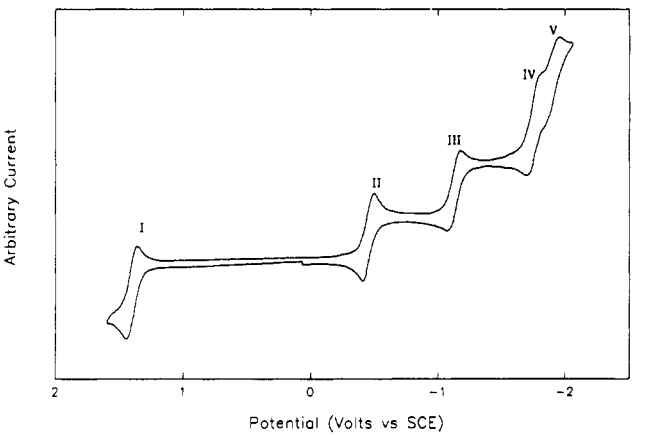

Figure 2. Cyclic voltammogram of $[Ru(bpy)_2(bqdi)]^{2+}$ complex in dry acetonitrile containing 0.1 M $TBAPF_6$. Potentials are referenced to SCE.

(49) Hansch, C.; Leo, A.; Taft, R. W. *Chem. Rev.* **1991**, *91*, 165.
(50) Lever, A. B. P. *Inorg. Chem.* **1990**, *29*, 1271.

Table II. Redox Potentials of $[Ru(bpy)_2(R_2\text{-bqdi})]^{2+}$ Complexes[a]

R	Ru^{III}/Ru^{II} (I)	bqdi/sqdi (II)	sqdi/opda (III)	bpy/bpy⁻(1) (IV)	bpy/bpy⁻(2) (V)	E_1[b]	$\Sigma\sigma_p$
4,5-$(NH_3^+)_2$							1.20
4-NO_2[c]	1.57	0.08	−0.69	−1.62	−1.86	0.38	0.78
4,5-Cl_2	1.50[d]	−0.28	−0.96	−1.75	−2.19[e]	0.33	0.45
H	1.37	−0.45	−1.13[e]	−1.70[d]	−1.94[d]	0.28	0.00
4,5-$(NH_2)(NH_3^+)$							−0.06
4,5-Me_2	1.32	−0.56	−1.21	−1.77	−1.94[d]	0.25	−0.34
4,5-$(OMe)_2$	1.15	−0.73	−1.26	−1.74[e]	−1.86[e]	0.16	−0.54
4,5-$(NH_2)_2$	0.83	−0.94[d,f]	−1.43[e]	−1.78[e]	−2.01[d,f]	0.01	−1.32

[a] Obtained in 0.1 M $TBAPF_6$ solutions in acetonitrile; potentials in V vs SCE. [b] See text for comments on these values; also see ref 48. [c] Monosubstituted at the 4 position. [d] Irreversible. [e] Quasi-reversible. [f] Peak potential.

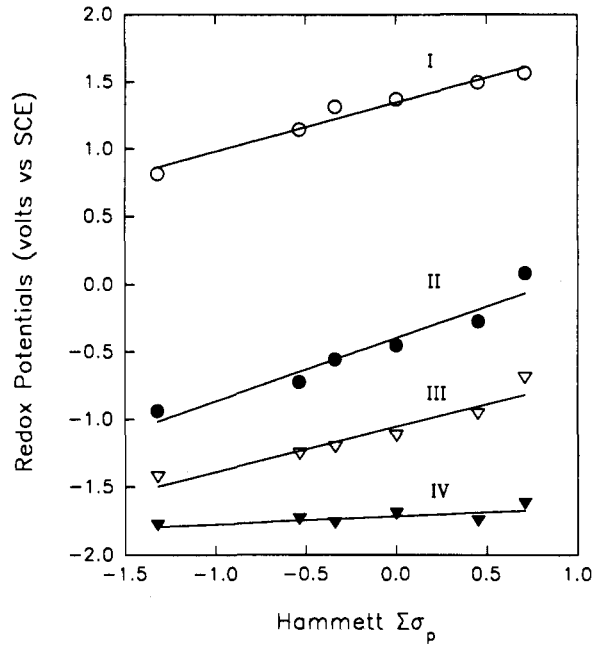

Figure 3. Substituent dependence of the redox potentials of the R_2-bqdi complexes (V vs SCE). The equations of the lines are as follows (values in parentheses are standard deviations and R = regression coefficient): (I) Ru^{III}/Ru^{II}, $E_{1/2} = 0.36\ (\pm0.035)\Sigma\sigma_p + 1.35\ (\pm0.024)$, $R = 0.982$; (II) R_2-bqdi/R_2-sqdi, $E_{1/2} = 0.47\ (\pm0.065)\Sigma\sigma_p - 0.40\ (\pm0.045)$, $R = 0.964$; (III) R_2-sqdi/R_2-opda, $E_{1/2} = 0.33\ (\pm0.053)\Sigma\sigma_p - 1.06\ (\pm0.037)$, $R = 0.952$; (IV) bpy/bpy⁻(1), $E_{1/2} = 0.059\ (\pm0.027)\Sigma\sigma_p - 1.72\ (\pm0.019)$, $R = 0.733$.

C. Electronic Spectra. The electronic spectral data and band assignments for all complexes discussed in this paper are listed in Table III.

(1) *o*-Benzoquinone Diimine Species, $[Ru(bpy)_2(R_2\text{-bqdi})]^{2+}$. The spectrum of a typical bqdi complex shows three low-energy charge-transfer bands (Figure 4) whose assignments have been discussed.[18] Band 3 usually appears as a shoulder of moderate intensity (ϵ = 5000–8000 $cm^{-1}\ M^{-1}$) on the high energy side of band 4, and its peak is resolved in complexes having more strongly electron-withdrawing substituents. It lies in a region where the rR spectrum of the related $[Ru(bpy)_2(o\text{-benzoquinone})]^{2+}$ complex[8] confirms the Ru → π*(1) bpy transition to occur. Further evidence for this assignment comes from the previously described relationship between the Ru^{III}/Ru^{II} redox potential and the energy of this transition, specifically[52]

$$h\nu[Ru \rightarrow \pi^*(1)bpy] = 0.65E[Ru^{III}/Ru^{II}] + 2.0\ (eV) \quad (1)$$

This relationship is expected if the HOMO, which is involved in the redox process, is also the orbital from which the charge-transfer transition originates. The HOMO, in this case, is either the a_1 or $2a_2$ level since the b_2 should be stabilized below the former by strong interactions with the bqdi ligand. Using eq 1 and couple I (Table II), there is a good agreement between observed and calculated energies of this transition; thus, band 3 is specifically assigned to Ru $a_1,2a_2 \rightarrow \pi^*(1)$ bpy. The Ru $1b_2 \rightarrow \pi^*(1)$ bpy transition must occur at an energy that ranges from 3000 to 8000 cm^{-1} higher than that of the Ru $a_1,2a_2 \rightarrow \pi^*(1)$ bpy transition. This value is estimated by subtracting the energy of band 5 (assigned below) from that of band 4. Such a transition has not been observed but may be hidden beneath stronger, adjacent bands.

A transition from the metal to a second bipyridine orbital, $\pi^*(2)$ bpy, occurs at an energy that is approximately 8000 cm^{-1} higher than that of band 3 and is often obscured by the base of an intense ligand-centered $\pi \rightarrow \pi^*$ transition. The Ru → $\pi^*(2)$ bpy transition, labeled band 2, is best resolved in the complexes having strongly electron-donating substituents and can be used to estimate the energy of the $a_1,2a_2 \rightarrow \pi^*(1)$ bpy transition when the latter is poorly resolved.

Band 4 is assigned to a transition from the b_2 to the $2b_2^*$ LUMO of the complex[18] on the basis of its relatively high intensity, given that transitions from a_1 or $2a_2$ will be weak due to poor overlap. Resonance Raman excitation profiles plotted for the 599-cm^{-1} (R = 4,5-Cl_2) and the 620-cm^{-1} (R = H) vibrations show that there is only one electronic transition within the envelope of band 4. Although isotopic substitution is needed to unequivocally identify this vibration, it is very likely to have considerable ν(Ru–N) character.[53] Higher frequency vibrations, e.g. bqdi or bipyridine ligand C=C and C=N, are not enhanced (Figure 5).

Since the intensity of an enhanced vibration is proportional to the square of the displacement and the square of the frequency of the vibration, i.e.

$$I_i \alpha \Delta_i^2 \omega_i^2$$

the lack of significantly enhanced vibrations near 1000–1600 cm^{-1}, where C=C and C=N stretches occur, provides strong evidence that their displacements are very small compared with that of the lower frequency Ru–N(diimine) stretch. Thus band 4 has very little charge-transfer character and is essentially a transition localized in the Ru–N(diimine) bond; i.e. a $\pi \rightarrow \pi^*$ transition involving this bond.

Band 4, which is unusually narrow, is skewed Gaussian[54] in shape, being 30–50% broader on the high-energy side, probably due to vibronic coupling and to overlap with the adjacent band 3. For discussion purposes, the bandwidth at $1/e$ height of this transition was obtained by doubling the measured half-bandwidth at $1/e$ height from the center of the band to lower energy.

It is not clear whether band 5 comprises one or two transitions, but in some instances the shape of the band suggests the presence of two transitions of similar energy (Figure 4). The band is very weak and by analogy to the assignments given for the spectrum of $[Cl(NH_3)_4Os(Hpz)]^{2+}$ by Magnuson and Taube[41] is assigned to the symmetry-allowed but overlap-forbidden transitions Ru $a_1,2a_2 \rightarrow 2b_2^*$ (LUMO) metal to ligand charge transfer (MLCT).

(a) Substituent Dependence. The energies of bands 3–5 are all dependent upon the bqdi substituent as shown in Table III and Figure 6. Generally, as the substituent becomes more electron-withdrawing, band 3 blue shifts and band 5 red shifts, both to a significant degree and both linearly with respect to the Hammett $\Sigma\sigma_p$ parameter. In acetonitrile solutions, band 4 follows a nonlinear dependence with a much smaller variation. Specifically, the energy of band 4 increases with $\Sigma\sigma_p$ from diamino ($\Sigma\sigma_p$ = −1.32; E = 18 100 cm^{-1}) to unsubstituted ($\Sigma\sigma_p$ = 0.00; E = 19 450 cm^{-1}) but falls as $\Sigma\sigma_p$ becomes even more positive as, for example,

(51) Masui, H.; Lever, A. B. P. To be submitted for publication.
(52) Dodsworth, E. S.; Lever, A. B. P. *Chem. Phys. Lett.* **1986**, *124*, 152.
(53) Mallick, P. K.; Danzer, G. D.; Strommen, D. P.; Kincaid, J. R. *J. Phys. Chem.* **1988**, *92*, 5628.
(54) Reimers, J. R.; Hush, N. S. *Inorg. Chem.* **1990**, *29*, 3686.

Table III. Electronic Spectra of Complexes[a] (cm^{-1})

$[Ru(bpy)_2(R_2\text{-bqdi})]^{2+}$ Complexes

R	$\pi \rightarrow \pi^*$ *o*-phenylene band 1	Ru d $\rightarrow \pi^*$ (1) bpy band 3	$b_2 \rightarrow 2b_2^*$ band 4	Ru $a_1,2a_2 \rightarrow 2b_2^*$ band 5
4,5-$(NH_3^+)_2$[b]		25 670 (3.73)	19 700 (4.32) (Δ3200)[c]	11 050 (2.36) (Δ6500)
4-NO_2[d]	35 840 (4.57)	24 040[e] (3.90)	18 980 (4.31) (Δ2850)	11 750 (2.49) (Δ4300)
4,5-Cl_2	35 720 (4.62)	23 760 (3.75)	19 030 (4.40) (Δ2750)	12 640 (2.07) (Δ3700)
H_2	35 650 (4.56)	22 810 (3.84)	19 440 (4.30) (Δ2850)	13 300 (2.74)
H_2[f]	35 540	22 730	19 490 (Δ2750)	13 290
4,5-$(NH_2)(NH_3^+)$[g]		22 620 (3.85)	18 800 (4.43) (Δ3050)	13 750 (2.66) (Δ5600)
4,5-$(CH_3)_2$	35 470	22 230 (3.90)	19 180 (4.40) (Δ2600)	13 700 (2.33) (Δ3900)
4,5-$(OCH_3)_2$	35 100	22 910 (3.85)	18 850 (4.49) (Δ2200)	15 000 (2.40) (Δ4800)
4,5-$(NH_2)_2$[h]	34 620	21 100 (4.04)	18 120 (4.57) (Δ1850)	15 600 sh

$[Ru(bpy)_2(R_2\text{-sqdi})]^+$ Complexes[i]

R	Ru d $\rightarrow \pi^*$(2) bpy band 7	Ru d $\rightarrow \pi^*$(1) bpy band 8	$b_2 \rightarrow 2b_2^*$ band 9	Ru $a_1,2a_2 \rightarrow 2b_2^*$ band 10
4-NO_2[d]	33 000 sh	21 960 (4.07), 24 200 sh	15 400 (4.24) (Δ2600)[c]	12 370
4,5-Cl_2	31 150 sh	21 000 (4.07)	15 350 (4.16) (Δ1650)	12 300
H_2	29 070 (3.91)	23 200 (3.88), 22 100 sh, 20 100, 19 400 sh	16 000 (4.05) (Δ2050)	11 100
4,5-$(CH_3)_2$	28 500 (3.93)	22 500 sh, 21 900 (3.93), 19 850 (4.02), 19 100 sh	16 150 (4.02) (Δ2300)	und
4,5-$(OCH_3)_2$[j]	29 600	21 980, 21 000, 28 000 sh	16 250 (Δ3000), 19 490, 19 080 sh	und

$[Ru(bpy)_2(R_2\text{-opdaH}_2)]^{2+}$ Complexes[k]

R	$\pi \rightarrow \pi^*$ *o*-phenylene band 11	Ru d $\rightarrow \pi^*$(2) bpy band 12	Ru d $\rightarrow \pi^*$(1) bpy band 13
4-NO_2[d,l]	34 370	30 090	21 790 sh, 20 840
4,5-Cl_2	34 500	32 400 sh	21 200
H_2	34 350 (4.40)	30 000 sh (3.62)	20 900 (3.73)
H_2[f]	und	und	20 530
4,5-$(CH_3)_2$	35 000 est	29 650	20 750
4,5-$(OCH_3)_2$	34 450	32 000 sh	20 750
4,5-$(NH_2)_2$	34 500	31 600	20 550

$Ru(bpy)_2(R_2\text{-opda})$ Complexes[j]

R	Ru d $\rightarrow \pi^*$(2) bpy band 15	Ru d $\rightarrow \pi^*$(1) bpy band 16	$opda^{2-} \rightarrow \pi^*$(1) bpy LLCT band 17
4-NO_2[d]	27 320	18 890	13 980, 13 000[m]
4,5-Cl_2	26 820[j]	18 490[j]	
4,5-Me_2	28 100[j]	18 700[j]	

[a] Spectra were obtained in acetonitrile except where otherwise stated. Log (ϵ) in parentheses. For band numbering, see figures. und = undetermined. Band 5 corresponds roughly with the difference in potential between couples I and II (Table II) (see text). These values are as follows: 4-NO_2, 11 750; 4,5-Cl_2, 14 150; H, 14 700; 4,5-$(CH_3)_2$, 15 100; 4,5-$(OCH_3)_2$, 15 100; 4,5-$(NH_2)_2$, 14 150 cm^{-1}. [b] Dissolved in concentrated H_2SO_4. [c] Bandwidths at $1/e$ of height, in parentheses. [d] Monosubstituted at 4 position. [e] Identified in spectrum recorded at 77 K; at room temperature this absorption is obscured by a nitro-related transition at 25 600 cm^{-1}. [f] Dissolved in water. [g] Dissolved in dilute 3 M HCl(aq). [h] Band 2, Ru d $\rightarrow \pi^*$(2) bpy, may be identified in this complex at 30 120 (4.11) cm^{-1}. [i] Spectra obtained in acetonitrile containing 0.3 M TBAP by controlled-potential reduction of the bqdi species (see text). Where sqdi (or opdaH$_2$) spectra are not reported for a specific species, this is generally due to the instability of the reduced species. [j] Isosbestics were lost halfway through electrolysis. Data were obtained from the last spectrum before loss of isosbestics. [k] Except where indicated, obtained by dissolving the isolated complex in acetonitrile. [l] Obtained in 5% HOAc in acetonitrile by Zn/Hg reduction of the NO_2-bqdi species. [m] Tentative assignment.

the nitro substituent ($\Sigma\sigma_p$ = +0.78; E = 19 000 cm^{-1}). The bandwidth of band 4 generally increases with $\Sigma\sigma_p$; however, the data points deviate from the best fit line in such a way that the deviations parallel the peculiar substituent dependence of the transition energy (see further discussion below).

In aqueous acidic media, the amino groups in the R = NH_2 species can be protonated, causing bands 3 and 4 to blue shift, while band 5 red shifts (Table III). A sigmoidal titration curve (Figure 7) of the absorption intensity of band 4 as a function of pH allows one to estimate the pK_a value of the complex; it is found to be 0.52 ± 0.1.

In 50% sulfuric acid the spectrum is further shifted and the complex is now apparently diprotonated. Certainly, a fit of the band energies to $\Sigma\sigma_p$ is excellent for all three transitions if diprotonation is assumed; and hence a value of $\Sigma\sigma_p$ = 1.2 is then accorded to the substituents on this species.[49]

Data are also reported for the monoprotonated species recorded in 3 M aqueous HCl. The energies of bands 3–5 also fit the substituent dependence line fairly well assuming $\Sigma\sigma_p$ = –0.06 for the sum of NH_2 and NH_3^+, with slight deviations probably due to the aqueous solvent (Figure 6).

(b) Solvatochromism. The diamino- and dichloro-substituted complexes, having substituents at the near extremes of the experimentally obtained $\Sigma\sigma_p$ values, show similar solvent dependences of their charge-transfer bands (Table IV). The energy of band 3 correlates linearly with the donor number of the solvent, DN,[55] red shifting as DN increases (4,5-Cl_2, slope = –56 cm^{-1}/DN, regression coefficient (R) = 0.96; 4,5-$(NH_2)_2$, slope = –32 cm^{-1}/DN, R = 0.97). This result indicates that charge is donated from the solvent to the benzoquinone diimine end of the complex, possibly through hydrogen bonding to the imine protons of the quinonoid ligand.

As shown by the slopes of the linear correlations, the solvent sensitivity of band 3 is greater for the dichloro complex than the diamino complex. This may be due to the reduced hydrogen-bonding acidity of the Cl_2-bqdi ligand at the imine protons of the diamino complex, causing weaker hydrogen bonding interactions of the protons with the solvent. It is also possible that the amine substituents of the diamino complex donate electron density directly to the solvent, but this is a minor contributing factor since there are no clear correlations with solvent hydrogen-bonding acidity.

Band 4 tends to shift to lower energies as the donor number of the solvent increases; however, the range of the shift is smaller than for band 3 and does not correlate well with DN. (4,5-Cl_2,

(55) (a) Gutmann, V. *Electrochim. Acta* **1976**, *21*, 661. (b) Hampe, M. J. *Ger. Chem. Eng.* **1986**, *9*, 251.

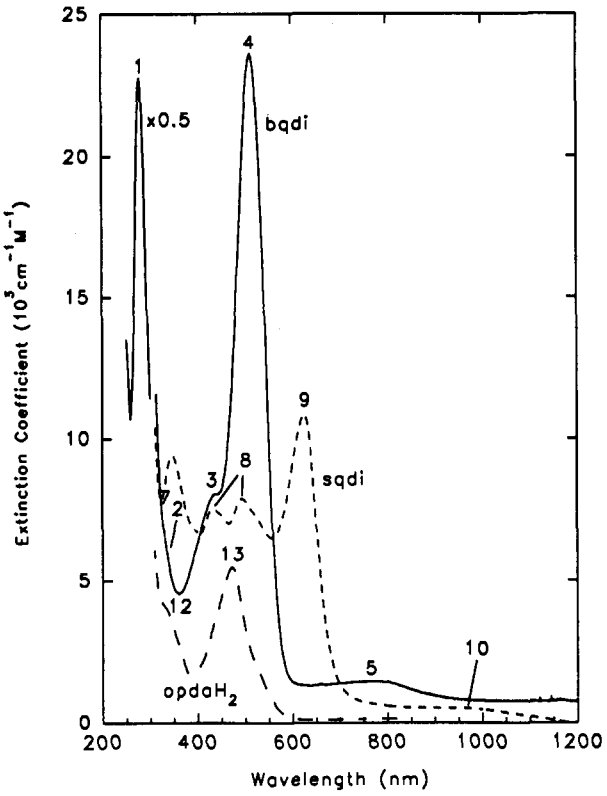

Figure 4. Typical spectra of the *o*-phenylene complexes in the three redox forms: (– –) $[Ru(bpy)_2(opdaH_2)]^{2+}$; (- - -) $[Ru(bpy)_2(sqdi)]^{+}$; (—) $[Ru(bpy)_2(bqdi)]^{2+}$. The data were obtained in acetonitrile. See Table III for assignments of identified transitions. Band 2 was only clearly identified in the $Ru(bpy)_2(NH_2)_2$-bqdi species spectrum.

slope = –12 cm^{-1}/DN, R = 0.78; 4,5-$(NH_2)_2$, slope = –4.9 cm^{-1}/DN, R = 0.47.) This is consistent with the conclusion that band 3 has significant MLCT character while band 4 has virtually no charge-transfer character.

The errors in determining the peak maxima of band 5 were large relative to the solvatochromic shifts; thus, for the dichloro complex it was difficult to ascertain whether band 5 correlates with DN. Such shifts could not be studied for the diamino complex because band 5 is obscured by band 4.

(2) *o*-Semiquinone Diimine Species, $[Ru(bpy)_2(R_2\text{-sqdi})]^{-}$. Controlled-potential reduction some 100 mV negative of couple II yields solutions of the R_2-sqdi species whose electronic spectra are reported in Table III and Figure 4. This reduction process shows Nernstian behavior for the $[Ru(bpy)_2(Cl_2\text{-bqdi})]^{2+}$ complex as is demonstrated by spectroelectrochemistry at various applied potentials through the redox wave,[56] and it is expected that the other complexes will exhibit similar behavior with the exception of the R = OMe and R = NH_2 species. These latter species undergo decomposition once a certain concentration of the R_2-sqdi species is generated.

Band 7, assigned to Ru $a_1,2a_2 \rightarrow \pi^*(2)$ bpy, shifts with substituent roughly parallel to the Ru $a_1,2a_2 \rightarrow \pi^*(1)$ bpy transitions of bands 8. The transitions of bands 8 are well separated in the species where R = OMe, Me, and H but are overlapping or poorly resolved for R = Cl and NO_2. The substituent dependence for bands 8 is shown versus the Hammett $\Sigma\sigma_p$ in Figure 8.

Resonance Raman spectra were recorded for R = Cl, in regions close to bands 8 and band 9, the Ru $b_2 \rightarrow 2b_2^*$ transition (see Experimental Section). Data for excitation close to bands 8 show the characteristic vibrational fingerprint of a Ru $\rightarrow \pi^*(1)$ bpy MLCT transition[8,57] (bands at 670, 1169, 1263, 1314, 1484, 1557, and 1604 cm^{-1}). These bands are absent from the spectrum obtained with excitation close to band 9. Instead skeletal modes of the sqdi ligand appear at 1475, 1351, and 1200 cm^{-1}, together

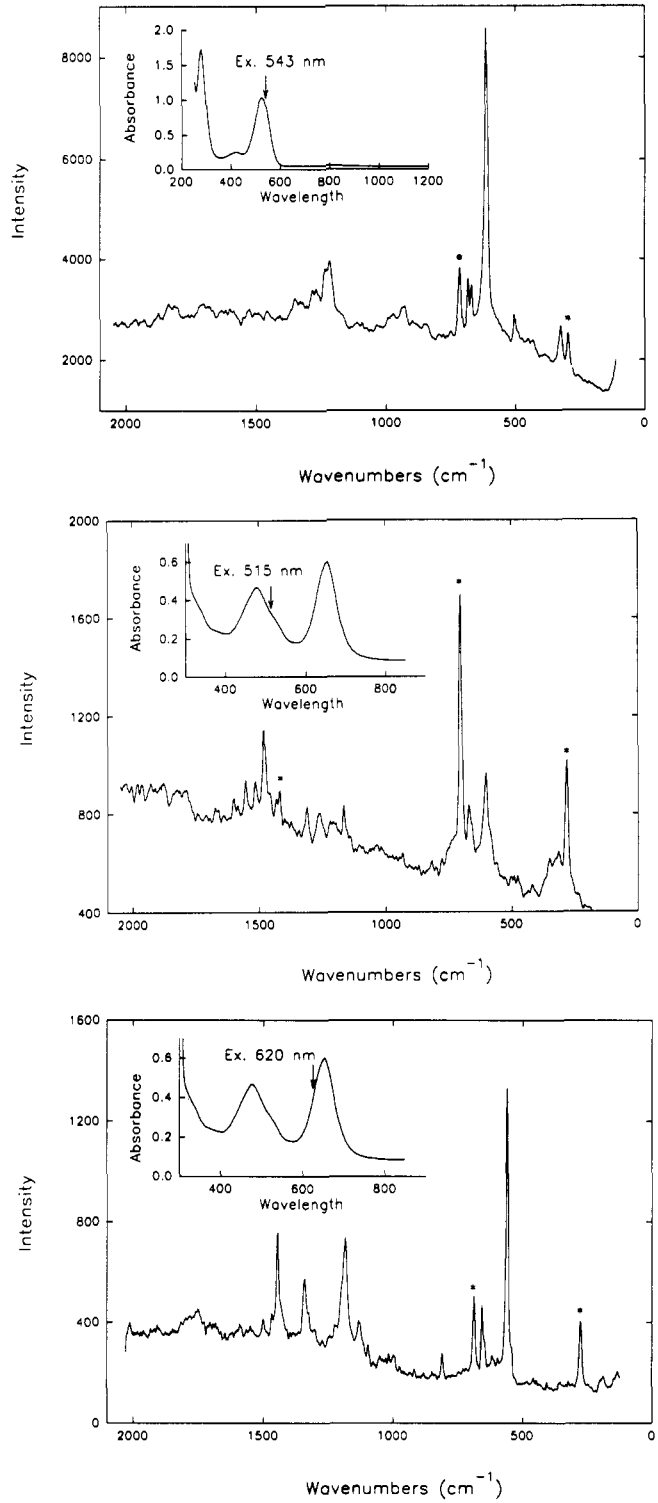

Figure 5. Resonance Raman spectra of the R_2-bqdi and R_2-sqdi complexes in CH_2Cl_2: (a) $[Ru(bpy)_2(Cl_2\text{-bqdi})]^{2+}$, excited at 543 nm; (b) $[Ru(bpy)_2(Cl_2\text{-sqdi})]^{+}$, excited at 515 nm; (c) $[Ru(bpy)_2(Cl_2\text{-sqdi})]^{+}$, excited at 620 nm. N.B.: In (b) the fairly prominent peak at 600 cm^{-1} is due to excitation of a small quantity of unreduced bqdi species. Asterisks denote solvent Raman lines.

(56) A plot of $\log\{(A_f - A)/(A - A_i)\}$ versus E_{app} (for $[Ru(bpy)_2(Cl_2\text{-bqdi})]^{2+}$ in acetonitrile) yields a linear correlation with a slope of 20.0 ($\sigma = \pm 0.4$) V^{-1}, a value of 16.95 V^{-1} being expected for a reversible one electron transfer process. Here, A is the peak absorbance of band 4 at the various applied potentials, E_{app}, and A_i and A_f are the limiting absorbances before and after reduction, respectively. The intercept yields an $E_{1/2}$ value of –0.23 V compared with –0.28 V in Table II.

(57) Balk, R. W.; Stufkens, D. J.; Crutchley, R. J.; Lever, A. B. P. *Inorg. Chim. Acta* **1982**, *64*, L49.

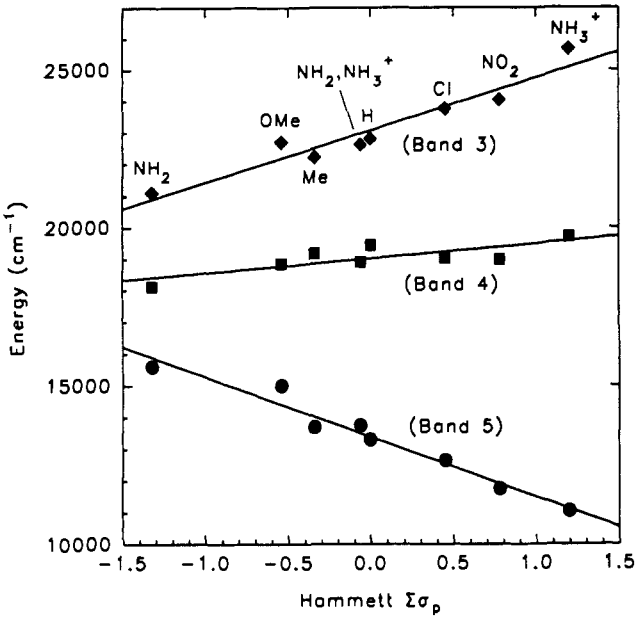

Figure 6. Substituent dependence of the various charge-transfer bands of the R_2-bqdi complexes. The data were mainly obtained in acetonitrile except for the 4,5-NH_2,NH_3^+ and 4,5-$(NH_3^+)_2$ species, which were obtained in 3 M HCl and concentrated H_2SO_4, respectively.

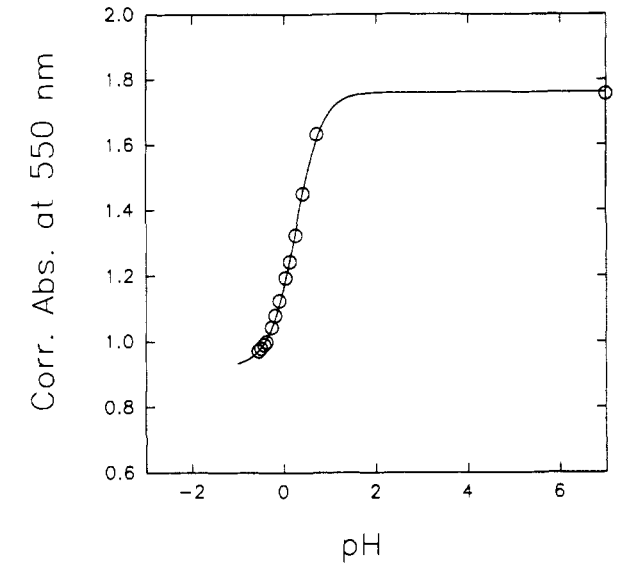

Figure 7. Titration of $[Ru(bpy)_2((NH_2)_2\text{-bqdi})]^{2+}$ in water with concentrated HCl and following the intensity of band 3 (corrected for dilution). A datum collected in 25% sulfuric acid ($pK_a \approx -0.95$), wherein the species is believed to be diprotonated, yielded a value of 0.70 absorbance units in this figure.

with a strong band at 566 cm^{-1}, which likely involves ν(Ru–N) (sqdi). The relatively strong enhancement of the skeletal modes, with respect to the Ru–N stretching mode typifies significant charge transfer in this transition.[8] Furthermore, band 9 behaves as an MLCT transition, generally shifting to the red with increasing acceptor character of the substituent.

Band 10, an ill-defined weak and broad transition centered near 900 nm, may be analogous to the forbidden Ru $a_1,a_2 \rightarrow 2b_2^*$ transition (band 5) in the bqdi oxidation state.

(3) Diamine Oxidation State Species, $[Ru(bpy)_2(R_2\text{-opdaH}_2)]^{2+}$. Since the diamine ligand has no low-lying empty π^* orbitals, no charge-transfer transitions involving the ligand and the metal are observed in the visible region. The visible absorption spectrum is then dominated by two Ru → bpy bands, band 12 (Ru $a_1,2a_2 \rightarrow \pi^*(2)$ bpy) and band 13 (Ru $a_1,2a_2 \rightarrow \pi^*(1)$ bpy) (Figure 4). The dependence of band 13 on the Hammett $\Sigma\sigma_p$ value is shown

Table IV. Solvatochromism of $[Ru(bpy)_2(R_2\text{-bqdi})]^{2+}$ (R = Cl, NH_2) (cm^{-1})[a]

		R = Cl			R = NH_2	
solvent	DN[b]	band 3[c]	band 4[d]	band 5[e]	band 4[d]	band 5[e]
CH_2Cl_2	0.0				21 900	18 200 (1820)
DCE	0.0				21 800	18 100 (1800)
MeCN	14.1	23 750	19 050 (2750)	12 750	21 250	18 200 (1810)
PC	15.1	23 650	19 000 (2600)	12 700	21 350	18 000 (1820)
Me_2CO	17.0	23 550	19 000 (2720)	12 200	21 300	18 100 (1820)
EtOAc	17.1	23 500	19 050 (2800)	13 450	21 100	18 200 (1740)
H_2O	18.0	23 650	19 050 (2740)	12 450	21 350	18 200 (3580)
MeOH	19.0	23 400	19 050 (2670)	12 550	21 150	18 200 (1910)
EtOH	20.0	23 200	18 950 (2550)	12 900	21 150	18 150 (1830)
THF	20.0	23 450	19 000 (2720)	12 300	20 950	18 050 (1880)
DMF	26.6	23 000	18 850 (2860)	12 950	20 900	18 000 (1860)
DMA	27.8	23 000	18 900 (2820)	12 800		
DMSO	29.8	22 860	18 850 (2670)	12 300	20 900	17 900 (1930)
EtCOMe		23 550	19 000 (2690)	12 850	20 900	17 950 (1840)
n-BuOH		22 500	19 000 (2810)			
n-PrOH		23 150	19 000 (2690)	12 650		
HOAc					21 400	18 150 (2200)

[a] Abbreviations are those commonly used. Note: PC = propylene carbonate and DCE = 1,2-dichloroethane. [b] Donor number.[54] [c] Ru $a_1,2a_2 \rightarrow \pi^*(1)$ bpy. Values in parentheses are half-bandwidths at $1/e$ of peak height. [d] $b_2 \rightarrow 2b_2^*$. [e] Ru $a_1,2a_2 \rightarrow 2b_2^*$.

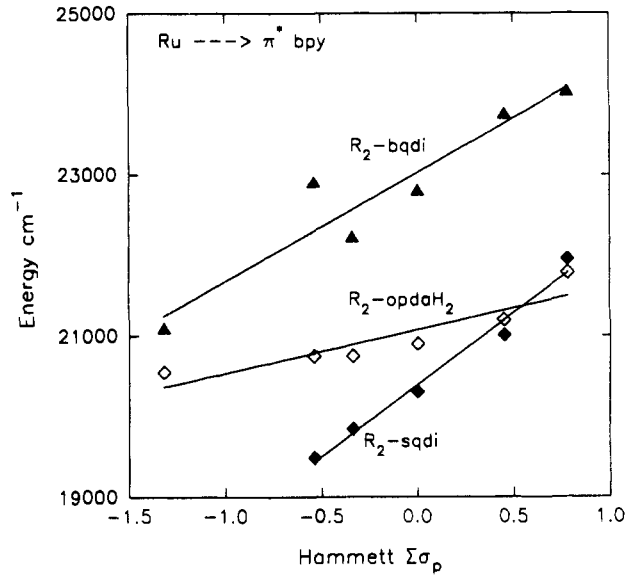

Figure 8. Plots of the Ru → $\pi^*(1)$ bpy transition energies as a function of Hammett $\Sigma\sigma_p$ for each redox form of the *o*-phenylene complexes. For the R_2-sqdi plot, the lower energy Ru $a_1,a_2 \rightarrow \pi^*(1)$ bpy band maximum was used where splitting of these transitions was observed.

in Figure 8. Additionally, there is a $\pi \rightarrow \pi^*$ transition (band 11) of the bipyridine ligands in the UV region which has been omitted from Figure 4 for clarity.

These data were obtained from samples of the isolated diamine complexes. Controlled-potential reduction of the bqdi species in aprotic solvents negative of the sqdi/opda redox couple yields the diamide versions of these species for R = NO_2 and to some extent, with slow decomposition, the R = Cl and R = Me species. With the softer diamide ligand, the Ru $a_1,2a_2 \rightarrow \pi^*(1)$ bpy (band 16) and the Ru $a_1,2a_2 \rightarrow \pi^*(2)$ bpy (band 15) transitions shift to the red, relative to the other opdaH_2 species, even though the 4-NO_2-opda and 4,5-Cl_2-opda ligands contain acceptor groups.

Consideration of the data shown in Figure 8, where the Ru → $\pi^*(1)$ bpy transition energy is plotted against $\Sigma\sigma_p$ for each oxidation state of the *o*-phenylene ligand, shows that this transition is strongly dependent upon substituent in both the bqdi and sqdi oxidation states but much less so in the fully reduced opdaH_2 state. Evidently in this last case, the sp^3-hybridized NH_2 groups interrupt the π-conjugation of the ruthenium atom with the ligand. The marked dependence for the sqdi oxidation state demonstrates

that even though these systems are believed to be less mixed than the bqdi oxidation state, the π-back-donation is still substantial.

D. Bonding Description. Recently Carugo et al.[40] analyzed the metal–nitrogen bond lengths of a large range of *o*-phenylenediamine complexes as a function of their oxidation state. They noted that these species do not generally yield charge localized structures and therefore cannot be characterized as having a formal oxidation state but rather a state between two of the three possibilities. They argued that it is possible to identify the net oxidation state of such a species from an analysis of the deviation of all the bond lengths from standard bond lengths for the opdaH_2 and bqdi ligands. In this manner, they characterized the [Ru(bpy)$_2$(H_2-bqdi)](PF_6)$_2$ species, whose structure is known,[26] as effectively containing Ru^{III} bound to the sqdi anion. For clarity of discussion, we will refer to this species as formally containing the bqdi ligand and most of the discussion which follows refers specifically to the bqdi oxidation state, except where specific reference to the other oxidation states is made.

The behavior of these bqdi complexes may be understood on the basis of essentially 50:50 metal–ligand mixing in the b_2 and $2b_2$* orbitals and less mixing in the a_1 and $2a_2$ orbitals such that the latter may be considered primarily metal in character. This model is consistent with the MLCT substituent behavior of band 5 (Ru a_1,$2a_2$ → $2b_2$*) as it shifts to lower energy with stronger acceptor groups (Figure 6). Further, the model is compatible with the blue shift of band 3 (Ru a_1,$2a_2$ → π*(1) bpy) with increasing acceptor character of the bqdi ligand (Figure 6) and with the lack of substituent dependence of band 4 (b_2 → $2b_2$*) since the orbitals involved have a mixed molecular orbital description.

(a) Mapping of Orbital Energy Levels with $\Sigma\sigma_p$ (Figure 9; Table V). One may roughly map the molecular orbital energies in the bqdi oxidation state species as a function of Hammett $\Sigma\sigma_p$ values by using experimentally obtained transition energy data. Such a map, however, neglects configurational interaction and includes reorganization energies and is, therefore, not a precise MO picture, but these effects should be reasonably independent of substituent for a given transition, and trends in the orbital energies should be fairly accurate.

Thus, Figure 9 is constructed in the following manner. The redox process corresponding to the bipyridine reduction, couple IV, has essentially no dependence upon the bqdi substituent; thus, the π*(1) bpy orbital can be used as an internal marker against which all other orbital energies may be referenced. The a_1,$2a_2$ levels (assumed degenerate) of the parent bqdi species (R = H) are assigned an energy of zero. These levels shift in concert with band 3, the Ru a_1,$2a_2$ → π*(1) bpy transition. Adding the energy of band 5 to the a_1,$2a_2$ levels yields the energy of $2b_2$*. Subtracting the energy of band 4 from the $2b_2$* level yields the energy of b_2, while subtracting the energy of the bqdi π–π* transition from that of $2b_2$* yields, approximately, the energy of a_2.

The substituent dependencies for the first oxidation and the first reduction potentials should be related to those in Figure 9, since they involve the a_1,$2a_2$ and $2b_2$* orbitals, respectively. However redox potentials describe the total free energy change in the redox process, i.e. a sum over all orbitals. The substituent dependence of this energy change will be largely determined by that of the orbital primarily involved in the redox process but must, for a metal-centered process, for example, also involve other metal orbitals, especially valence orbitals of comparable energy.

The open squares on the $2b_2$* line in Figure 9 show the variation of couple II as a function of $\Sigma\sigma_p$, setting the species with R = H to fit onto the $2b_2$* line. There is a good correspondence between the two slopes, though that of the redox potential is slightly larger, probably due to a contribution from the substituent dependence of the b_2 orbital which is greater than that of $2b_2$*.

The substituent dependence of couple I is also shown in Figure 9, normalized to a potential of zero for R = H. Its slope is considerably greater than that of the a_1,$2a_2$ line, being 2900 $cm^{-1}/\Sigma\sigma_p$ compared with 1630 $cm^{-1}/\Sigma\sigma_p$ for a_1,$2a_2$. This difference can be explained by contributions from the other valence orbitals to the substituent dependence of the redox potential. For example, averaging the slopes of the a_1,$2a_2$, and b_2 levels predicts a redox potential slope of 2410 $cm^{-1}/\Sigma\sigma_p$, closer to that observed. This value would be further increased by a contribution from the $2b_2$* dependence.

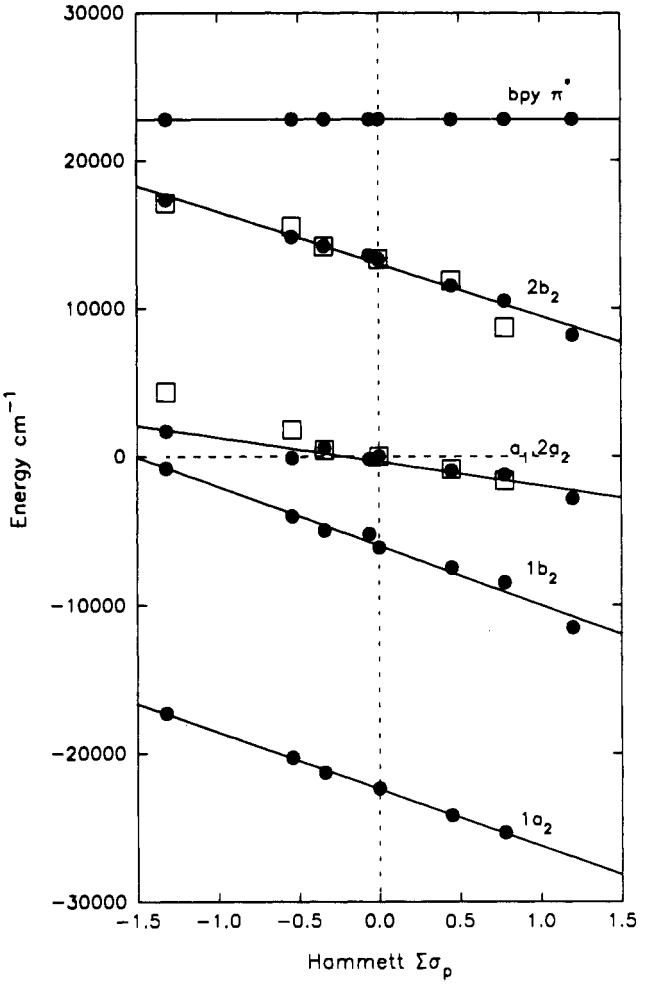

Figure 9. Plots of the trends in molecular orbital energies of the R_2-bqdi complexes as a function of $\Sigma\sigma_p$ (see text). The energies are referenced to a fixed π*(1) bpy orbital, and the a_1,$2a_2$ orbitals of the R = H species have been arbitrarily set to zero. The square symbols represent experimentally obtained redox potentials as described in the text.

Table V. Regression Analysis for Data Shown in Figure 9

MO/couple	slope (std dev) (cm^{-1})	const (std dev) (cm^{-1})	no. of points	regression coeff
a_2	−3830 (70)	−22400 (110)	6	0.99
b_2	−3970 (240)	−6000 (500)	8	0.99
a_1,$2a_2$	−1630 (210)	−350 (440)	8	0.95
$2b_2$*	−3500 (170)	13000 (360)	8	0.99
couple I[a]	2840 (290)	10900 (490)	6	0.98
couple II[a]	3730 (460)	−3300 (770)	6	0.97

[a] Redox potentials converted to wavenumbers 1 eV = 8065 cm^{-1}.

Comparisons of this type may help to clarify the electronic structures of these species, but they are simplified in the sense that one cannot necessarily assume that the ordering of the d orbitals or identity of the HOMO is the same in the Ru^{III} species as it is in the Ru^{II} species; thus, it may not be meaningful to talk of a redox process involving removal of an electron from a specific orbital.

The almost parallel dependence of b_2 and $2b_2$*, following from the relatively small dependence of band 4 upon $\Sigma\sigma_p$, implies considerable mixing between the ruthenium d(yz) and ligand π*

orbital (back-donation). Numerical assessment of the degree of mixing, based upon earlier treatments by Vlcek,[58] de la Rosa et al.,[59] and Mines et al.[60] indicates essentially 50:50 mixing of ligand and metal orbital, when ligand and metal redox processes behave in a parallel fashion upon a perturbation such as variation of substituent. However, such treatments are approximate and are only strictly applicable where the mixing is small.

The essentially parallel dependence of the $1a_2$, $1b_2$, or $2b_2^*$ orbital energies (Table V) may be fortuitous. The $1a_2$ orbital's lower energy and lower polarizability should cause the orbital to be less substituent dependent than the $2b_2^*$ orbital, while its lesser degree of mixing with the metal, compared with $2b_2^*$, should have the opposite effect. The sum of these two effects has probably resulted in the parallel dependence of these three orbitals.

(b) Reorganization Energy Contributions—Band 5. For a MLCT transition in a general complex, $M^{II}X_5L$, one may write[52]

$$h\nu = E[M^{III}/M^{II}](L) - E[L/L^-](M^{III}) + \chi_i + \chi_o \quad (2)$$

$$h\nu - \Delta E[\text{redox}] + \chi_i + \chi_o \quad (3)$$

where $\chi_i + \chi_o$ are respectively the inner (vibrational) and outer (solvent) reorganization energies and $E[L/L^-](M^{III})$ signifies the reduction potential for ligand L bound to a M^{III} center. In practice only $E[L/L^-](M^{II})$ (the ligand reduction potential when it is attached to a central M^{II} ion) can be observed, where

$$E[L/L^-](M^{III}) = E[L/L^-](M^{II}) + q \quad (4)$$

q is a positive number which effectively incorporates a collection of differential solvation energy terms and a Coulombic term. We can then write

$$\Delta E[\text{redox}]' = E[L/L^-](M^{II}) - E[M^{III}/M^{II}](L) \quad (5)$$

$$h\nu = \Delta E[\text{redox}]' - q + \chi_i + \chi_o \quad (6)$$

It is almost invariably true that $\Delta E[\text{redox}]'$ underestimates $h\nu$ such that the reorganization energy terms are larger than q.[4,61] The situation for band 5 is unusual in that $\Delta E[\text{redox}]'$ (couple I – couple II) *overestimates* $h\nu$ (band 5) by some 1000–1500 cm^{-1} for all R, except R = NO_2 and R = OMe, where the agreement is exact. Thus, if the theory is formally applied, $q > \chi_i + \chi_o$. Since band 5 shows considerable charge-transfer character, there is no compelling reason for believing that the reorganization energy is small. This would lead one to conclude that perhaps q is unusually large, consistent with 50:50 mixing of ligand and metal valence orbitals. Less mixing should lead to a smaller dependence of ligand reduction potential on the oxidation state of the metal.

(c) Reorganization Energy Contributions—Band 4. A value for $\Delta E[\text{redox}]'$, appropriate for band 4, cannot be derived from electrochemistry since the loss of an electron from the b_2 orbital is not directly observed. Hence, an analysis similar to that performed on band 5 is not possible.

The small dependence of band 4 upon $\Sigma\sigma_p$ has indicated that this transition has little charge-transfer character in keeping with the rR spectra reported above. However, there is an apparent pattern when these data are cross-correlated with bandwidths and ν(Ru–N) as shown in Figure 10. Since band 4 transitions are narrow, the errors on their energies are quite small.

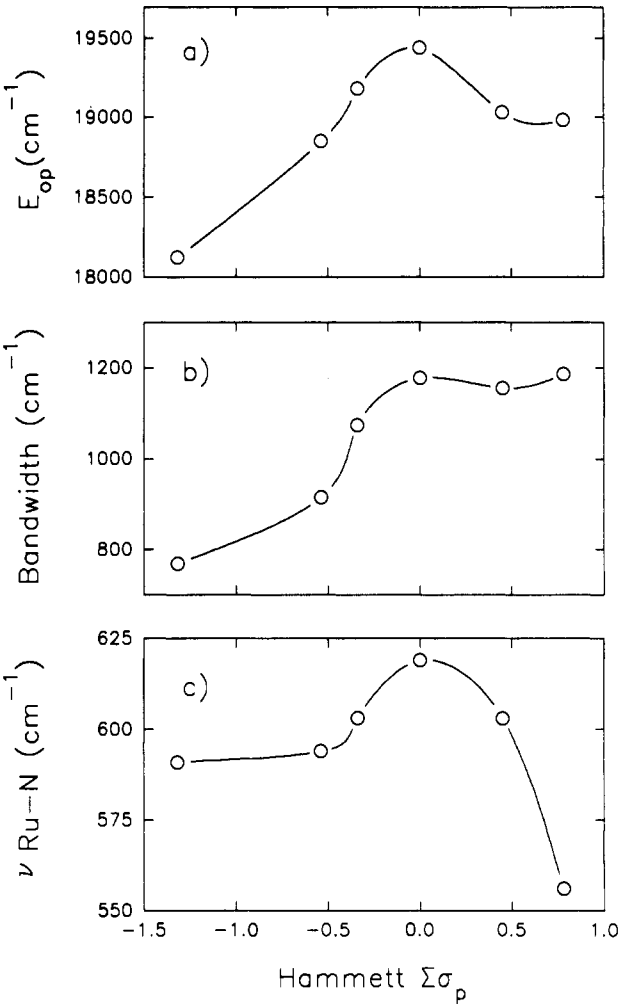

Figure 10. Plots of (a) the energy of band 4, (b) the bandwidth of band 4, and (c) the ν(Ru–N) FTIR data as a function of Hammett $\Sigma\sigma_p$ for the R_2-bqdi species. Electronic spectra were obtained from acetonitrile solutions while FTIR data were obtained from KBr pellets.

The bandwidth measured at $1/e$ of the height of the band, $2\sigma^2$, is related to the displacements, Δ_k, and frequencies, ω_k, of the kth vibrations coupled to the electronic transition via[62]

$$2\sigma^2 = \sum \Delta_k^2 \omega_k^2 \quad (7)$$

where the parameter Δ_k is a dimensionless measure of the distortion[62] in the metal–ligand bond. Since the inner reorganization energy can be written as a sum over $K_q\Delta_k^2$, where K_q is the force constant of the bond, the bandwidth and reorganization energy are closely related.

A strictly parallel dependence of the b_2 and $2b_2^*$ energy levels upon the Hammett $\Sigma\sigma_p$ parameter would predict no dependence of the energy of band 4 upon $\Sigma\sigma_p$ except due to reorganization energy. Thus we may seek to attribute the pattern in Figure 10 to reorganization energy variations with substituent. The narrowness of band 4 reflects the fact that distortion proceeds essentially along one coordinate (Ru–N) and that the frequency thereof is relatively small (approximately 600 cm^{-1}). Figure 10 shows that these parameters do behave in an overall parallel fashion with the energy of band 4, confirming that the small variations with $\Sigma\sigma_p$ do reflect variations in reorganization energy.

The behavior of band 4 in the R_2-bqdi species contrasts with that of the $b_2 \rightarrow 2b_2^*$ transition in the less mixed R_2-sqdi species (band 9), which, in its dependence upon $\Sigma\sigma_p$, is a more typical MLCT transition. However, the bandwidths of band 9 are

(58) Vlcek, A. A. *Electrochim. Acta* **1968**, *13*, 1063.
(59) de la Rosa, R.; Chang, P. J.; Salaymeh, F.; Curtis, J. C. *Inorg. Chem.* **1985**, *24*, 4229.
(60) Mines, G. A.; Roberts, J. A.; Hupp, J. T. *Inorg. Chem.* **1992**, *31*, 125.
(61) Ghosh, P.; Chakravorty, A. *Inorg. Chem.* **1984**, *23*, 2242.
(62) Tutt, L.; Zink, J. I. *J. Am. Chem. Soc.* **1986**, *108*, 5830.

comparable to those of band 4 and the parallelism that exists between the transition energy and bandwidth in the R_2-bqdi complexes also occurs in the R_2-sqdi complexes. Note that the $R = NO_2$ species has both unusually large bandwidth and transition energy which do not follow the general trend to lower energies with increasing $\sum\sigma_p$. This species has lower symmetry than the disubstituted species, and it is possible that two transitions may lie under the band envelope.

Conclusions and Summary. If the mixing in the b_2 and $2b_2^*$ levels in these species is approaching 50:50 $d(yz) + \pi^*$(bqdi), then there is a significant formal Ru^{III}sqdi contribution to the Ru^{II}bqdi ground state, in agreement with the conclusion of Carugo et al.[40] In such a case there will be little substituent dependence of the $b_2 \rightarrow 2b_2^*$ transition energy, as is the case here, and the small variations which are observed (Figure 10) reflect variations in reorganization energy, χ_i, from one complex to another.

The apparent ambiguity between the description as Ru^{II}bqdi or Ru^{III}sqdi can now be rationalized in terms of the specific orbitals involved in the various electronic transitions and the strong mixing. The $a_1,2a_2$ orbitals are mainly metal in character so that transitions therefrom, specifically band 3, Ru $a_1,2a_2 \rightarrow \pi^*(1)$ bpy, and band 5, Ru $a_1,2a_2 \rightarrow 2b_2^*$, appear strongly MLCT in character and have normal, i.e. not especially narrow, bandwidths. With increasing electron acceptor character of the diimine ligand, electron density is drained off the metal center and the $a_1,2a_2$ orbitals are stabilized. The direction of shift of the MLCT transitions is dictated by the dependence of the metal and terminal MO's on substituent, the latter being assumed zero for $\pi^*(1)$ bpy and being progressively stabilized with increasing acceptor ability for $2b_2^*$.

Band 4 ($b_2 \rightarrow 2b_2^*$) involves a transition between levels which have roughly 50% metal and 50% ligand character so that it is not a charge-transfer transition at all but rather an internal transition of the total molecular complex, a situation discussed previously by Kaim.[63] It may be called a metal–ligand to metal–ligand transition, MLML, to distinguish it from an internal transition of the ligand alone. It has characteristics similar to a $\sigma \rightarrow \sigma^*$ transition in a metal–metal-bonded species, L_nML_n, such as being strongly localized in the molecule, having bonding to antibonding character and narrow bandwidth, and being absent from the spectra of the monomeric counterparts. Accordingly, we have also observed that photochemical excitation may cause metal–ligand dissociation in these species, but this has not yet been studied in detail.

Finally, the formal values for the E_L parameter[50] noted in Table II are approximate since couple I is not a pure Ru^{III}/Ru^{II} couple but contains a contribution from the ligand. The effect of "filtering out" the ligand contribution is likely to reduce the overall range of E_L values for this series of complexes.

Acknowledgment. We are indebted to the Natural Sciences and Engineering Research Council (Ottawa) and the Office of Naval Research (Washington, D.C.) for financial support. We also thank Prof. William J. Pietro for access to, and guidance in use of, the Spartan software, Prof. D. J. Stufkens and Dr. Th. L. Snoeck for the resonance Raman data, Xiuyu Tai and Lori Payne for technical support, and the Johnson-Matthey Co. for the loan of ruthenium trichloride.

(63) Kaim, W.; Gross, R. *Comments Inorg. Chem.* **1988**, *7*, 269.